In-Situ Thickness Method of Measuring Thermo-Physical Properties of Polymer-Like Thermal Interface Materials

R. Andrew Smith, Richard J. Culham
Micro-Electronics Heat Transfer Laboratory
University of Waterloo, Waterloo, Canada

Abstract

A critical property in understanding and accurately predicting the thermal resistance of polymer-like thermal interface joints in micro-electronic cooling applications is the bulk thermal conductivity of Thermal Interface Materials (TIMs). A unique experimental test stand was developed and validated which accurately measures the in-situ thickness of a TIM sample in a vacuum during thermal resistance testing. The system has a resolution capability of $\pm 1.0 \mu m$ and is designed in such a manner as to continuously measure the true relative deflection of a TIM sample taking into account any mechanical and/or thermal deflections of the entire test stand. The data and analysis demonstrate that applying the current American Standard Test Method (ASTM) ASTM D 5470 without accounting for in-situ thickness deviations can result in over estimating the bulk thermal conductivities for these types of materials by as much as 40%. These types of errors in fundamental material properties can cause the over-prediction of thermal heat flux in a system and an under-prediction of the temperatures of the system.

Keywords

ASTM D 5470, Thermal Resistance, Thermal Interface.

Nomenclature

A	apparent contact area [mm^2]
ASTM	American Society for Testing and Materials
BRM	Bulk Resistance Method
E	Young's modulus [MPa]
ISTM	In-Situ Thickness Method
k	thermal conductivity [W/m K]
m	slope of ASTM data [K mm/W]
P	pressure [MPa]
PSD	Position Sensitive Detector
Q	rate of heat transfer [W]
R	thermal resistance [K/W]
RMS	Root Mean Square
r	specific thermal resistance [mm^2 K/W]
R^2	Pearson correlation coefficient
T	temperature [°C, K]
TIM	Thermal Interface Material
t	thickness [mm]
x	linear distance in x plane [mm]
y	linear distance in y plane [mm]

Greek Symbols

α	conversion factor = 1000 [mm/m]
Δ	change in value
ε	compression per unit thickness$\times$100% [%]
ω	calculated uncertainty
Γ	PSD manufacturing error

Subscripts

contact	contact between two surfaces
f	final
i	initial
in-situ	measurement taken in place while under testing
int	y axis intercept for ASTM D 5470
gap	absence of surface to surface contact
heat source	source of heat
heat sink	receiver of heat
l	lower
lf	lower final
li	lower initial
mfg	manufacturer's specifications
u	upper
uf	upper final
ui	upper initial
1,2,3	relating to bodies 1,2 or TIM samples 1, 2, 3

Superscripts

$'$	effective

1. Introduction

It is common knowledge in many branches of industry and science that for any two solid surfaces in contact, the true area in contact will only be a small fraction of the apparent contact area. As two bodies are slowly moved close together at very low loads, they will initially make molecule-to-molecule contact at just a few discrete points. Surrounding these areas of molecule-to-molecule contact will be areas of no contact where there are 'gaps' between the two bodies. This behavior arises from the fact that at the microscopic level, solid surfaces are not perfectly flat but in fact resemble a continuous three-dimensional array of peaks and valleys. The end result is that the true area in contact at a joint between two surfaces under load is significantly less than the apparent area in contact.

In the study of heat transfer phenomena the microscopic behavior of surfaces in contact creates a resistance to the transfer of heat between the two bodies. The thermal resistance at the surface is created by the constriction of the heat flow to the small areas of true molecular contact between the two surfaces and the presence or absence of conduction, convection or radiation at areas of no contact or gaps. The magnitude of the resistance is affected by several parameters including the geometry or roughness of the surfaces, the deformation characteristics or hardness of the surfaces, the total load being supported by the surfaces in contact, and the type of gas or absence of gas in the gaps between the areas of true contact.

A typical thermal engineering problem in the micro-electronics industry will consist of removing heat across a surface from a silicon chip heat source and into a highly conductive heat sink. In order to reduce the negative effect of thermal resistance at the interface between the two surfaces, it is common practice to utilize a soft and thin material of higher conductivity than air to reduce the resistance to heat flow by increasing the surface area in contact at the interface and increasing the effective conductivity of the surface interface joint.

A useful analogy used in the analysis of these types of thermal conduction problems is to exploit the similarity between the diffusion of heat and the diffusion of electrical charge through a conductor [1]. A simple TIM joint is shown as a thermal resistance circuit in Figure 1. The scale of the surface roughness has been exaggerated for illustration purposes. The resistance circuit in Figure 1 can be expressed mathematically as

$$R_j = \left(\frac{1}{R_{contact_1}} + \frac{1}{R_{gap_1}} \right)^{-1} + R_{TIM} + \left(\frac{1}{R_{contact_2}} + \frac{1}{R_{gap_2}} \right)^{-1} \quad (1)$$

In the micro-electronics industry, as components become smaller and thermal density increases, considerable effort is devoted to increasing the transfer of heat across interfaces such as those in Figure 1, in order to reduce the temperatures of sensitive micro-electronic components. To a thermal designer, effectively evaluating the thermal conductivity of a particular TIM is critical. Thermal conductivity is an experimentally measured property of a material and is reported for thin, thermally conductive solid electrical insulation materials according to the instructions set out by ASTM D 5470.

ASTM D 5470 [2] is designed to be a general guide to the research scientist and application engineer. The standard describes a system which consists of a heat source and a heat sink each with two temperature measurement devices installed. The tests are performed at a load of 3.0 ± 0.1 MPa. At very high loads, it is expected that a typical TIM material will be soft enough to conform almost fully to the interfaces, thus reducing the interfacial contact resistances, and as a result the TIM thermal resistance will dominate the joint resistance.
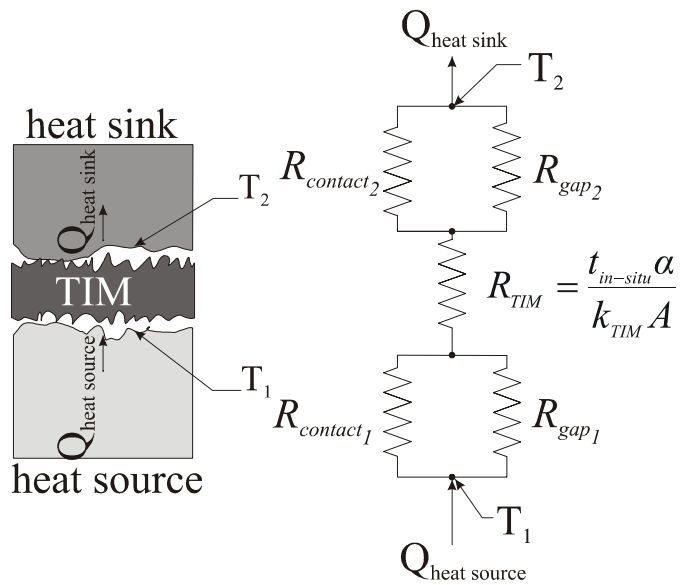

Figure 1. TIM Joint Resistance Circuit

The testing is performed at an average specimen temperature of 50°C to simulate a typical micro-electronics heat transfer interface and at steady state where steady state, is defined as a drift of less than ± 0.2K between two successive temperature samples taken at 15 minute intervals.
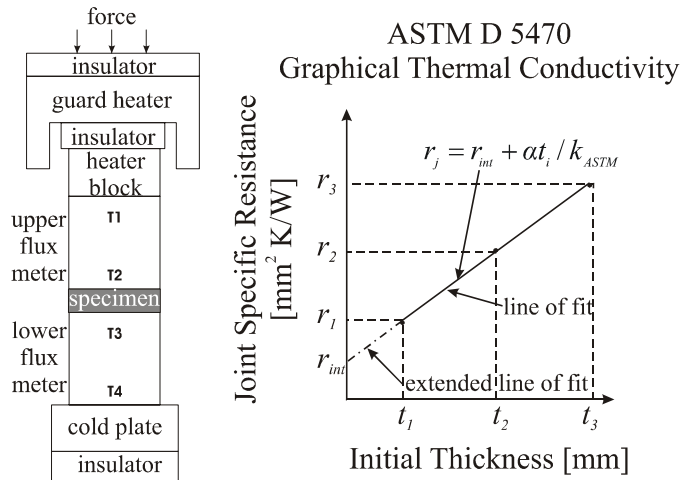

Figure 2. ASTM D 5470 Schematic

Referring back to Equation 1, if the interface contact and gap resistances are treated as a total constant contact resistance defined as r_{int}, and multiplying by the area to give specific thermal resistance, the thermal resistance circuit can be simplified to

$$r_j = r_{int} + r_{TIM} = r_{int} + \frac{\alpha t_i}{k_{ASTM}} \quad (2)$$

The temperature at each interface is estimated by extrapolating linearly the two temperature measurements from the body of each block to the interface, as shown in Figure 3.

The heat transfer rate through the sample is measured using either a reference calorimeter or by measuring the applied electrical heater power. Using guard heaters and insulation reduces heat transfer losses to the surroundings by convection and conduction.
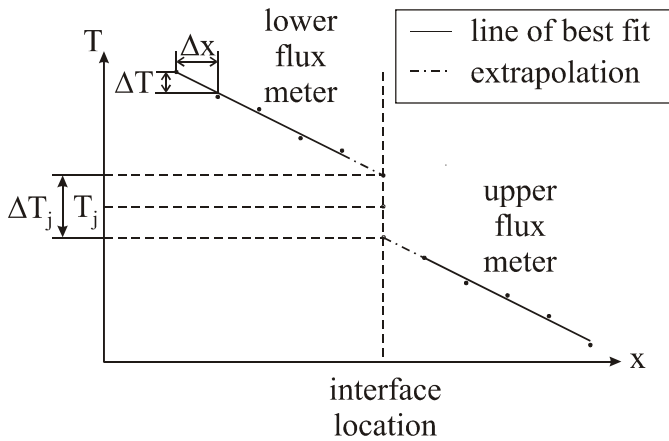
Figure 3. Estimation of Interface Temperatures

The test is performed on multiple thicknesses or layers of the material of interest, and a plot of measured specific thermal resistance on the *y*-axis versus sample thickness on the *x*-axis is generated, as shown in Figure 2. The assumption is that a sample of double the thickness will have double the resistance to heat flow and similarly for triple the thickness, or in other words that the relationship between thickness and specific thermal resistance is linear. It is assumed that if multiple thicknesses are used that the additional resistance between each material interface is insignificant.

The TIM thickness for each test is measured at room temperature and at zero load condition prior to the thermal resistance testing. A line of best fit using least mean squares is generated through the specific thermal resistance data. The inverse of the slope of the line of best fit results in the thermal conductivity of the material. This is illustrated mathematically in Equation 2 with r_{int} giving the *y* intercept and $1/k_{ASTM}$ representing the slope.

An excellent overview of the ASTM D 5470 test method is presented by DeSorgo [3]. DeSorgo comments that the sample thickness should be accurately measured during the test in order to produce accurate results, but that the current ASTM D 5470 standard does not specify this requirement. As well, in an article published by Lasance [4], Lasance notes that the proliferation of misleading data on thermal properties of TIMs causes much irritation by vendors and users alike. Lasance notes that round-robin tests using ASTM D 5470 have demonstrated a repeatability error between labs of 20 to 40%.

Parihar and Wright [5] investigated the thermal contact resistance of SS304 – silicon rubber – SS304 joints under light loads. The experimental program was run in air using a single calibrated linear variable differential transducer to measure the deflection of the deadweight loading platform and related to in-situ sample deformation. Parihar and Wright concluded that for common silicon rubbers, the interface resistance is about 25% of the total resistance with the majority of the resistance to heat transfer coming from the bulk resistance of the material. Parihar and Wright did not comment on the resolution, accuracy or repeatability of the in-situ thickness system.

Rauch [6] investigated three phase change thermal interface materials. Rauch measured the deflection of the guard heater relative to the cooling unit using a single precision dial indicator. Rauch observed that the reduction in measured compound thickness resulted in a proportional decrease in thermal resistance.

Solbrekken et al. [7] described the development of a tool to predict thermal interface performance. One of the key components of this system was the ability to measure in-situ thickness of the materials being tested. The test apparatus has 1mm marks in the heating and cooling calorimeter blocks at a distance of 400μm from the calorimeter edge. Before the sample being tested is placed between the surfaces of the heating and cooling calorimeters, the distance between the two marks is measured with the faces of the blocks in direct contact. This will later be used as an initial zero point reference between the blocks. The physical measurement is made through a digital camera and software combination which had a resolution of ±75μm thus limiting the overall thickness measurement system to ±75μm. Solbrekken et al. note in their conclusions that although the interface tester has proven to be a useful tool as the demand for lower thermal resistance materials increases, the resolution of the tester will be significantly challenged.

In 2003, work was published by Prasher et al. [1] describing work on particle laden polymers. In this work, Prasher et al. describe measuring the in-situ thickness using a laser extensometer. The laser extensometer operates by sensing reflections from retroreflective strips applied to the heating and cooling rods. The strips are located 2.5mm from the end of each rod. These strips function as targets and the system determines the distances between the selected edges of the targets with a scanning laser beam. Prasher et al. report a repeatability of the extensometer of ±1.0μm and a resolution of ±1.0μm.

Savija et al.{9}/[10], developed a new technique for in-situ thickness measurement based purely on thermal data from thermal interface test experimental results called the simple Bulk Resistance Method (BRM). The basis of the technique is to measure the slope of the specific joint resistance data versus pressure, at pressures high enough to be sure that the contact resistance between the TIM and the contacting surfaces is minimal. Savija et al. assume linear deformation of the bulk material under load and use Hooke's Law to define an effective Young's modulus, E', and an in-situ thickness as shown in Equation 3.

$$t_{BRM} = t_i \left(1 - \frac{P}{E'} \right) \tag{3}$$

Savija et al. then use the linear calculation for in-situ thickness to predict a thermal conductivity by adjusting for in-situ deformation of TIM materials.

As indicated in Equation 2, the measured specific thermal resistance is directly proportional to the thickness of the sample used in the calculation, and as a result the in-situ thickness will directly impact the measurement of the bulk thermal conductivity of the TIM using the ASTM D 5470. Since it is desirable for TIMs to be manufactured as soft and pliable materials, it is not unusual for TIMs to exhibit significant deformation at the ASTM D 5470 specified test load of 3.0 ± 0.1 MPa. None of the literature reviewed described specific experimental evidence of the impact of material deformation of polymer-like thermal interface materials on the test results of the ASTM D 5470 method.

The purpose of this work is to provide evidence of the impact of in-situ thickness changes on the thermal conductivity relative to the ASTM D 5470 method and present a simple and inexpensive method of measuring in-situ thickness for an ASTM D 5470 test method approach.

Thermal conductivities are calculated using a similar approach to the ASTM D 5470 standard but substitute true measured in-situ thickness in place of initial thickness. Using the In-Situ Thickness Method (ISTM), Equation 2 can be rewritten as shown in Equation 4.

$$r_j = r_{int} + r_{TIM} = r_{int} + \frac{\alpha \, t_{in-situ}}{k_{ISTM}} \tag{4}$$

Thermal conductivities measured using ISTM and using the BRM method developed by Savija et al. [9]/[10] will be compared relative to values of thermal conductivity given by applying ASTM D 5470 and values provided by the manufacturers.

2. Experimental Program

The development of the base thermal test facility and test facility used in this work has been extensively described in work presented by Savija [11] and Culham [12]. A photograph and schematic of the system is presented in Figure 4 and Figure 5.

The entire system is highly automated. The user can select a desired interface temperature and a series of loads to process at that interface temperature. The control system will automatically set the linear actuator to the initial load, control the heaters to set the interface temperature, automatically calculate the thermal resistance, and ascertain steady state before cycling to the next load. Typically, a test incorporating 18 different load settings could take over 13 hours and only require 20−30 minutes of interaction by the user. The system maintains the mean temperature of the joint within ±5% (°C) of the desired set point and the pressure within ±1% (MPa) of the set point. Changes in joint temperature, heat rate, joint thermal conductivity, and joint thermal resistance are automatically monitored. When the ratio of the slope of the last ten values for all convergence parameters is not greater than 0.05%, then the system determined that steady state had been reached. All relevant data required is stored in text spreadsheet files, which can easily be viewed after the experiment.
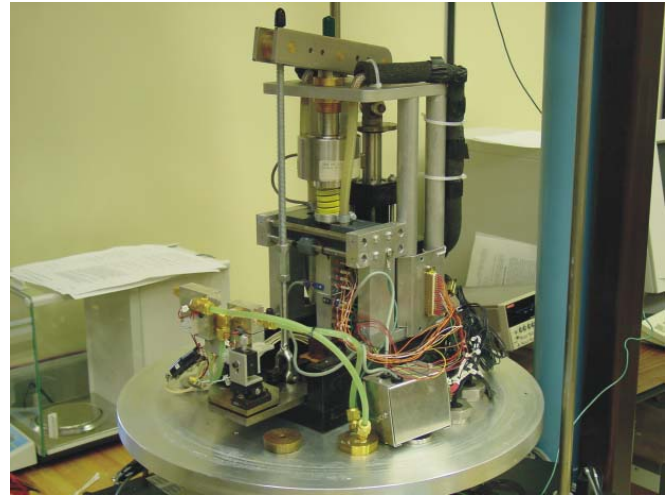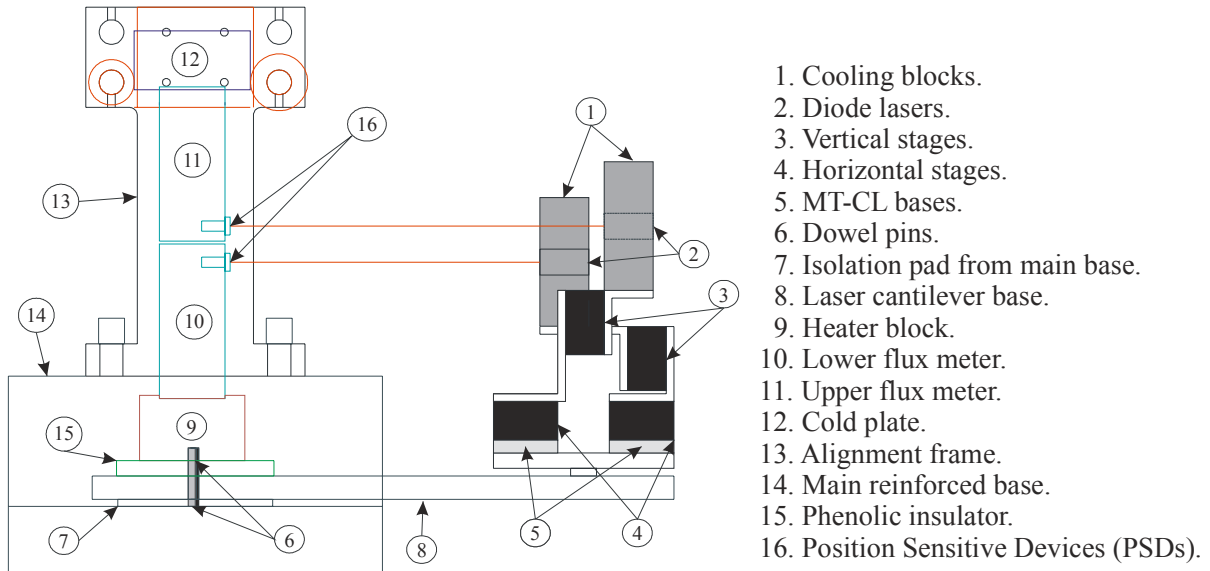

Figure 4. Test Stand Photograph

Three types of TIMs were tested: specifically, eGraf 1210, CHO-THERM 1671, and CHO-THERM 1674. All testing was done in a vacuum at an average interface joint temperature of 50°C and a load of 3.0 MPa.

The materials were cut into approximately 25mm × 25mm square test specimens and the initial thicknesses measured using a Mitutoyo outside micrometer. For tests where multiple layers were run, the initial thickness was measured with all layers stacked together. Specific care was taken to cut the samples slightly larger than the face of the flux meters. As well, particular care was taken not to touch the area within the sample being tested so as not to contaminate or damage the TIM surface. The faces of the aluminum flux meters were cleaned between tests using an acetone soaked soft wipe and were then blown clean with a zero residue canned compressed air cleaner known as Super Duster 134 from MG Chemicals.

The test sample was inserted into the opening between the flux meter faces using tweezers. Again using tweezers, the sample was carefully aligned to match the alignment of the upper and lower flux meters so that there was a uniform amount of test material protruding from the edges all the way around the flux meters. The cooling plate was carefully put into place on top of the upper flux meter and the alignment of the test column was checked and adjusted if necessary using the alignment jig. The alignment jig is an aluminum piece that was machined flat with a notch to allow for the position of the test sample. The alignment jig is used to align the lower flux meter with the upper meter as shown in Figure 6. This procedure seemed to provide better repeatability of in-situ thickness measurements.

1. Cooling blocks.
2. Diode lasers.
3. Vertical stages.
4. Horizontal stages.
5. MT-CL bases.
6. Dowel pins.
7. Isolation pad from main base.
8. Laser cantilever base.
9. Heater block.
10. Lower flux meter.
11. Upper flux meter.
12. Cold plate.
13. Alignment frame.
14. Main reinforced base.
15. Phenolic insulator.
16. Position Sensitive Devices (PSDs).

Figure 5. Schematic Layout of Test Stand

One of the key innovations of this test stand is the in-situ precision thickness system. Conceptually, the system is quite simple and consists of a pair of low powered diode lasers mounted to focus laser light on two semiconductor PSDs. One PSD is mounted on the upper calorimeter and the other on the lower calorimeter, with the centerline of each PSD approximately 10mm from the joint interface. As the sample material and flux meters deform due to thermal effects or mechanical loading, the system tracks the movement of the incident light on the surface of each PSD and determines the in-situ thickness as a function of the initial thickness of the sample and the differential thickness recorded by the PSDs.
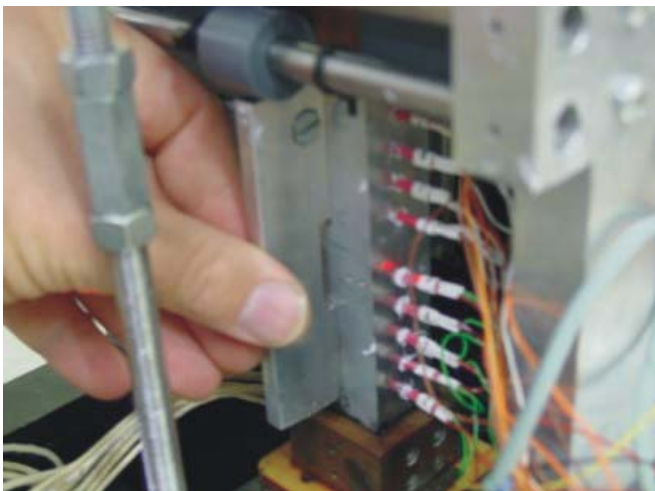

Figure 6. Alignment Jig in Use

The in-situ position measurement algorithm is:

1. Measure the sample TIM initial thickness, t_i, in length units of mm using a Mitutoyo outside digital micrometer at a pressure of 0.02MPa. The Mitutoyo micrometer has a mechanical clutch mechanism that, according to the manual, sets the applied pressure during measurement to 0.02MPa. The micrometer has one stationary platen and one movable platen which will rotate when it makes initial contact with the sample. Both platens are 20.0mm in diameter.

2. The sample TIM is then placed between the two flux meters and initial absolute position values are obtained from the PSDs at an apparent interface pressure of 0.02MPa, in units of mm for both upper and lower flux meters. These will be t_{ui} and t_{li} for the initial position of the laser beams on the upper and lower flux meter PSDs respectively.

3. During each data acquisition scan, the system uses outputs from the PSD signal processing circuit to calculate a final absolute position (positive or negative to the zero absolute position of the PSD) for the laser center of light location on each PSD. These will be t_{uf} and t_{lf} for the final position of the laser beams on the upper and lower flux meter PSDs respectively.

4. After each data acquisition scan, the system calculates a current in-situ thickness using the difference between the measured initial and final absolute position of each PSD mounted on each flux meter to give $t_{in-situ} = t_i - [\Gamma_u(t_{ui} - t_{uf}) + \Gamma_l(t_{li} - t_{lf})]$ where Γ_u and Γ_l represent correction factors to account for manufacturing errors in the upper and lower PSD sensors.

At the end of each test and after the sample has been removed, the final thickness is manually measured using the Mitutoyo outside micrometer and recorded. A photograph showing a TIM in place between the flux meters is shown in Figure 7. The components shown in the photograph are:

1. Lower PSD sensor.
2. Lower laser light incident on PSD sensor active area.
3. Lower flux meter.
4. TIM.
5. Upper laser light incident on PSD sensor active area.
6. Upper PSD sensor.
7. Upper flux meter.
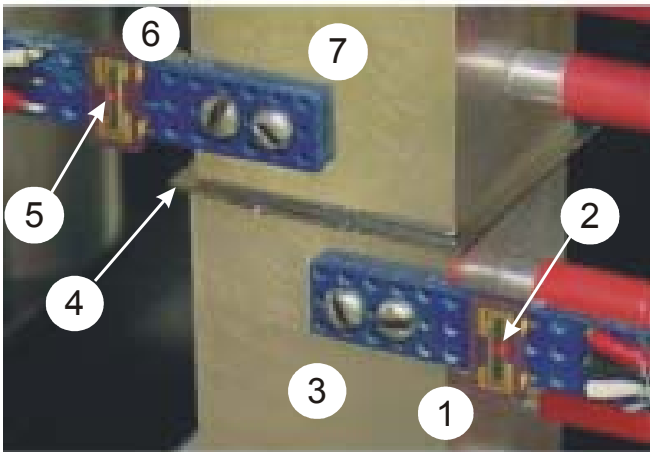
Figure 7 - PSD with Incident Laser Light

3. Analysis

Using the test procedure described above, specific thermal resistance test results were obtained for single, double and triple layers of the three TIMs at loads of between 0.0 and 6.5 MPa. Each individual test consisted of increasing and decreasing loads to accurately describe the full transition behavior of the thermal joint system during loading and unloading. Two independent samples were run for each sample thickness layer resulting in a total of six test results for each TIM. The first section that follows will discuss the in-situ thickness measurement results and the second section will detail the ASTM D 5470 results.

3.1. In-Situ Thickness of TIMs

The contact resistance test apparatus continuously measures the thickness of the sample during testing. As a result, it is possible to present normalized per cent strain data for each sample regardless of its initial thickness. In this way, it is possible to compare the deformation response of all six independent tests done on each TIM.

The independent variable of the chart is the apparent contact pressure as measured with the in-situ load cell. The dependent variable is the normalized strain data calculated as a percentage, as shown in Equation 5.

$$\varepsilon = \frac{t_i - t_{in-situ}}{t_i} \times 100\% \qquad (5)$$

The eGraf 1210 series material per cent strain results are presented in Figure 8. The data show an interesting trend with a significant increase in the rate of strain between loads of 1.0MPa and 4.0MPa. The rate of strain then slows at loads greater than 4.0MPa. It is clear that the unloaded material plastically deformed by almost 50%. This agrees well with final thickness measurements made on the material as shown in Table 1

The unloading data also demonstrate an interesting feature in that they show the material increasing in thickness between loads of 3.0MPa and 1.0MPa. It is believed that this behavior is as a result of the test stand structure straining at the higher loads and introducing this error into the measurements. Similar trends are seen in the data for both the CHO-THERM 1671 and 1674 materials.

Each data point is an average of the six samples, two samples each of 1, 2, and 3 layers. The horizontal range bars shown represent the maximum difference at each load between the individual per cent stress values recorded experimentally and the average per cent stress value calculated from all six data points.

The CHO-THERM 1671 material deformation is presented in Figure 9. It shows that the unloaded material has plastically deformed by only 6% compared to the 50% variation seen with eGraf 1210. This again agrees well with final thickness measurements made on the material using the hand-held Mitutoyo micrometer.

As shown in Figure 10, the stress versus strain for loading and unloading of CHO-THERM 1674 is more difficult to explain than the behavior of either CHOTHERM 1671 or eGraf 1210. The data seem to suggest that the material during loading does not deform at all, averaging 0% strain, and upon unloading, the material seems to increase in thickness with higher positive strains ending up at around 2%. Once again, this behavior is attributed to the non-linear straining of the test stand. The manually measured and in-situ values for final thickness agree well and are summarized in Table 1.

3.2. Thermal Conductivity Test Results

As described in the introduction, the thermal conductivity of a material can be obtained in a systematic manner by taking the inverse of the slope of the specific thermal conductivity versus initial thickness of multiple layers or thicknesses of the test material. The raw data used in this analysis are presented in Table 2. The actual plotted ASTM D 5470 data are summarized in Table 3 and plotted in Figure 11, Figure 12, and Figure 13 for eGraf 1210, CHO-THERM 1671, and CHO-THERM 1674 respectively.

A summary of the final thermal conductivity values comparing the methods of ASTM, ISTM, and BRM is presented in Table 4. The summary data illustrates that the ISTM system and the simple BRM methods of calculating the thermal conductivity both predict lower bulk thermal conductivities than the value calculated using the ASTM D 5470 method, which is expected since both of these methods account for the in-situ bulk material deformation, whereas the

ASTM D 5470 method does not.

In the case of eGraf 1210, the predicted thermal conductivity value using the ISTM approach is 38% lower than the value predicted using the ASTM D 5470 method. For the ISTM method, this lower conductivity appears to be related to the reduction in bulk thickness of the material at the 3MPa load used for the ASTM D 5470 method. The average measured strain using the in-situ measurement system at 3MPa was 35.9%. The simple BRM method predicts a higher thermal conductivity than the ISTM method, but a lower thermal conductivity than the ASTM D 5470 method. This is expected since the simple BRM method predicts a linear elastic in-situ thickness deformation. In effect, the simple BRM method under predicts the in-situ deformation of the eGraf 1210 and as a result, predicts a higher thermal conductivity than the ISTM method. As was indicated in the discussion of the eGraf 1210 data, the stress strain performance of the material is far from linear.

sample #	# layers	t_i [mm]	$t_{in\text{-}situ}$ @ 3.0 MPa [mm]	Mitutoyo t_f [mm]	ISTM t_f [mm]	final Mitutoyo strain [%]	ISTM final strain [%]
eGraf 1210							
1	1	0.260	0.167	0.150	0.141	42.3	45.9
2		0.257	0.171	0.147	0.135	42.8	47.4
3	2	0.515	0.326	0.293	0.275	43.1	46.5
4		0.513	0.329	0.281	0.257	45.2	49.8
5	3	0.774	0.514	0.435	0.405	43.8	47.7
6		0.804	0.483	—	0.376	—	53.2
CHO-THERM 1671							
1	1	0.432	0.395	0.405	0.404	6.2	6.5
2		0.415	0.390	0.395	0.382	4.8	8.0
3	2	0.849	0.784	0.801	0.800	5.7	5.8
4		0.854	0.788	0.789	0.800	7.6	6.3
5	3	1.243	1.184	1.140	1.200	8.3	3.5
6		1.258	1.163	1.175	1.182	6.6	6.0
CHO-THERM 1674							
1	1	0.296	0.303	0.287	0.287	3.0	3.0
2		0.291	0.294	0.286	0.284	1.7	2.4
3	2	0.575	0.578	0.573	0.570	0.3	0.9
4		0.585	0.589	0.577	0.583	1.5	0.4
5	3	0.873	0.878	0.860	0.870	1.5	0.4
6		0.872	0.870	0.859	0.863	1.5	1.0

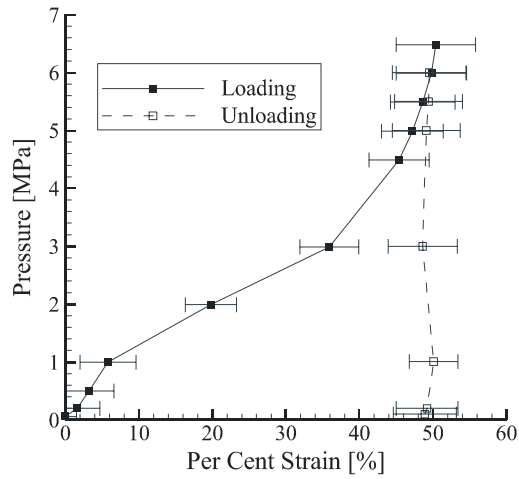**Table 1** Summary of Final Thickness Data

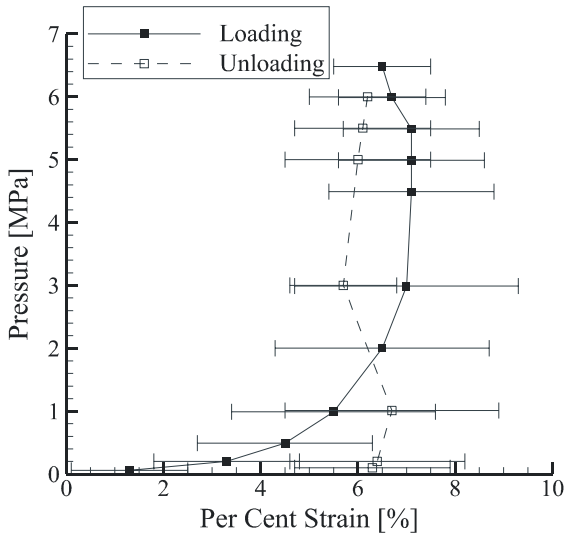**Figure 8.** Averaged Stress versus Strain, Multiple Layers, eGraf 1210

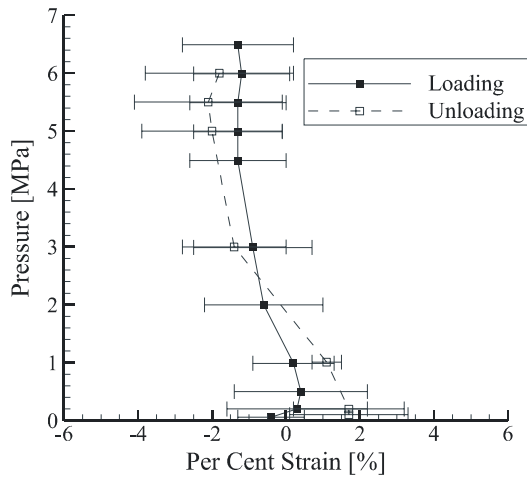**Figure 9.** Averaged Stress versus Strain, CHO-THERM 1671

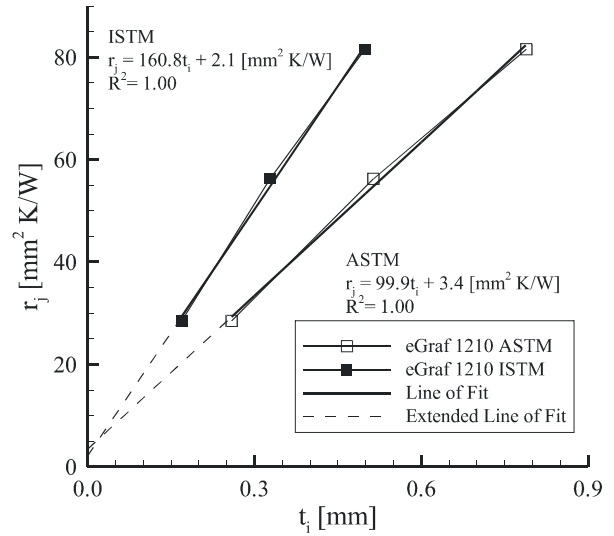**Figure 10.** Averaged Stress versus Strain, CHO-THERM 1674

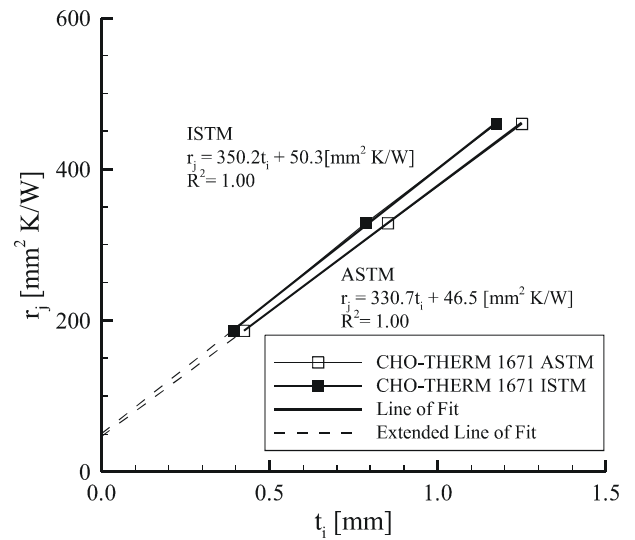**Figure 11.** eGraf 1210 ASTM D 5470

Figure 12. CHO-THERM 1671 ASTM D 5470

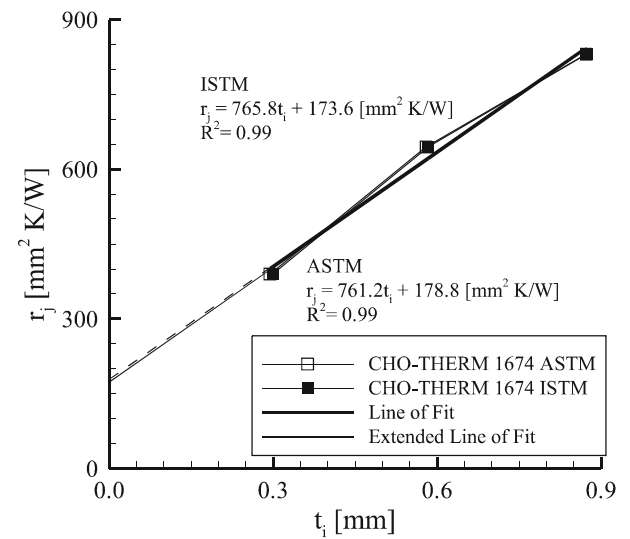**Figure 13.** CHO-THERM 1674 ASTM D 5470

Sample #	r_j [mm^{2}K/W]	E' [MPa]	k_{BRM} [W/m K]
eGraf 1210			
1	28.1	20.9	5.15
2	28.9	23.2	4.93
3	56.7	18.8	5.75
4	55.8	18.1	5.83
5	83.9	19.5	6.06
6	79.2	18.4	6.67
CHO-THERM 1671			
1	178.2	20.0	1.4
2	194.4	17.6	1.2
3	323.8	25.4	1.5
4	333.3	22.8	1.5
5	466.7	27.3	1.6
6	452.9	32.1	1.6
CHO-THERM 1674			
1	400.2	16.2	0.4
2	379.5	17.5	0.4
3	611.2	29.8	0.6
4	678.4	22.8	0.5
5	818.5	62.2	0.7
6	843.1	52.0	0.6

Table 2 Individual Thermal and BRM Data

		eGraf 1210	CHO-THERM 1671	CHO-THERM 1674
ASTM Method				
m_{ASTM}	[K mm / W]	99.9	330.7	761.2
r_{int}	[mm^2 K/W]	3.4	46.5	178.8
$1/m_{ASTM}$	[W / mm K]	0.0100	0.0030	0.0013
k_{ASTM}	[W / m K]	10.0	3.0	1.3
ISTM Method				
m_{ISTM}	[K mm / W]	160.8	350.2	765.8
r_{int}	[mm^2 K/W]	2.1	50.3	173.6
$1/m_{ISTM}$	[W / mm K]	0.0062	0.0029	0.0013
k_{ISTM}	[W / m K]	6.2	2.9	1.3

Table 3 ASTM D 5470 Summary Dat

	eGraf 1210	CHO-THERM 1671	CHO-THERM 1674
k_{ISTM} [W / m K]	6.2	2.9	1.3
k_{BRM} [W / m K]	8.2	2.2	0.8
k_{ASTM} [W / m K]	10.0	3.0	1.3
k_{mfg} [W / m K]	10.0	2.6	1.0
ε_{ISTM} @ 3 MPa [%]	35.9	7.0	-0.9
ε_{BRM} @ 3 MPa [%]	13.6	15.6	17.5

Table 4 Conductivity Summary Table

In the case of CHO-THERM 1671, the predicted thermal conductivity value using the ISTM approach is 3% lower than the ASTM D 5470 method. For the ISTM method, the lower conductivity appears to be mainly related to the reduction in bulk thickness of the material at the 3.0MPa load used for the ASTM D 5470 method. The average measured strain using the in-situ measurement system at 3.0MPa was 7%. The simple BRM method predicts a lower thermal conductivity than the ISTM method for CHO-THERM 1671. This is expected since the simple BRM method predicts a linear elastic in-situ thickness deformation whereas the ISTM method accounts for true measured bulk material deformation. In effect, the simple BRM method over predicts the in-situ thickness deformation of the CHO-THERM 1671 and as a result, predicts a lower thermal conductivity than the ISTM method.

In the case of CHO-THERM 1674, the predicted thermal conductivity value using the ISTM approach is the same as the ASTM D 5470 method. In this case, the measured ISTM per cent strain indicated that the material increased in thickness by 0.9% at a load of 3.0MPa which seems to be counter-intuitive. In fact, as was discussed in the stress-strain

analysis section, the measured strain results for this material were all within ±3% of the initial thickness, which is less than the total observed ISTM system error of ±3%. The simple BRM method predicts a lower thermal conductivity than the ISTM method for CHO-THERM 1674. This is expected since the simple BRM method predicts a linear elastic in-situ thickness deformation whereas the ISTM method accounts for true measured bulk material deformation. In effect, the simple BRM method over predicts the in-situ thickness deformation of the CHO-THERM 1674, and as a result predicts a lower thermal conductivity than the ISTM method.

In all cases, the Pearson correlation coefficient for the line of best fit for the ASTM D 5470 and ISTM data is almost exactly 1.00 which indicates there is excellent agreement between the line of fit and the experimental data. This validates both the experimental data and the assumption of linearity between specific thermal resistance and thickness made in the ASTM D 5470 approach.

3.3. Uncertainty

As described in the device specifications, the PSD devices have a resolution of ±1.0µm[13]. However, a more complete analysis is required to understand the ISTM measurement error for in-situ thickness and in-situ thermal conductivity. A full analysis was completed using the standard Root Mean Square (RMS) approach as presented in Holman [14]. The full analysis is presented in [15] and is summarized here.

The initial thickness is determined, as described earlier, by manually measuring the sample thickness using a digital outside micrometer from Mitutoyo. The uncertainty in calculated in-situ thickness is affected significantly by the overall uncertainty of the Mitutoyo outside micrometer. The micrometer has a stated uncertainty of ±5.0µm. The uncertainty in measured absolute position on the PSD itself is affected by the amount of current being generated in the device and the overall physical length of the sensing element. The uncertainty in the absolute position calculation on the PSD has been calculated as ±2.2µm. This results in an overall in-situ thickness uncertainty being calculated as ±5.5µm.

The ISTM bulk thermal conductivity is calculated by measurement of the in-situ thickness and in-situ specific thermal resistance value taken at 3.0MPa. Therefore, the uncertainty of the thermal conductivity is dependent on the uncertainty of the in-situ thickness, the thickness of the sample, and the specific thermal resistance value measured. The uncertainty for a single layer of material is presented in Table 5.

Material	T $\omega_{k_{ISTM}}$ [W/m K]
eGraf 1210	0.6
CHO-THERM 1671	0.2
CHO-THERM 1674	0.1

Table 5 ISTM Thermal Conductivity Uncertainty

A complete analysis of the thickness and thermal conductivity uncertainty should also include an analysis of the experimental error. Including the experimental error would somewhat increase the calculated uncertainties presented here. The experimental uncertainty could be estimated by performing a series of tests on materials of different thicknesses and thermal conductivities within the expected range of application. Each test would be repeated several times on new samples and an analysis of variance performed to understand the true gauge uncertainty contribution to in-situ thickness and thermal conductivity.

4. Conclusions

In summary, a successful effort was undertaken to develop a system capable of measuring in-situ strain with repeatability and reproducibility of approximately ±3% of the initial thickness of the material. Comparisons between the final manually measured thickness and the final measured in-situ thickness agreed well. This in-situ thickness was used to calculate the thermal conductivity of various TIM materials using the ASTM D 5470 approach. The in-situ measurement system has been developed with cost in mind and can be retro-fitted to existing guarded heater design test stands. A simplified cost summary with costs in $US is presented in Table 6.

Component	Qty	Cost [$US]	Total [$US]
Optima Precision Inc. model DLM 2303 − 650 diode laser.	2	81.62	163.24
Newport single axis stage with base.	2	122.43	244.86
Constant temperature bath.	1	2448.57	2448.57
Aluminum cooling blocks.	2	40.81	81.62
One-dimensional PSDs model S3931from Hamamatsu.	2	40.81	81.62
Hamamatsu C3683-01 signal processing circuit for a one-dimensional PSD.	2	1632.38	3264.76
		Total [$US]:	6284.66

Table 6 Cost Summary of Position Device

The ISTM method for calculating thermal bulk conductivity was compared to two other methods, specifically the ASTM D 5470 standard approach and the simple BRM method developed by Savija et al.[9]/[10]. It was found that in two of the three materials tested, the ISTM and the BRM method predict lower thermal conductivities for the bulk material than the ASTM D 5470 standard approach. The differences between the ISTM and simple BRM method thermal conductivities appear to be related to the fact that the ISTM method is able to account for non-linear plastic in-situ thickness deformations of the bulk material, whereas the

simple BRM assumes a linear elastic deformation of the material, which causes the method to either over or under predict the in-situ thickness and thermal conductivity. This is a known limitation of the simple BRM method and indicates the main advantage of the ISTM method over the simple BRM method since many polymeric TIMs will exhibit non-linear in-situ thickness variation. A second limitation of the simple BRM method is that it does not account for the constant of specific thermal resistance related to the test stand itself, r_{int}, which can significantly effect the calculated thermal conductivity value.

Through the course of this work, many electro-mechanical changes to the experimental test apparatus became obvious that may improve the performance of the system in the future. These changes are fully documented in.[15]

Acknowledgments

References

1. . Frank P. Incropera and David P. DeWitt, Fundamentals of Heat and Mass Transfer, Fourth Edition, Wiley, New York, 1996.
2. ASTM D 5470 Standard Test Method for Stead-State Thermal Transmission Properties of Thin Thermally Conductive Solid Electrical Insulation Materials, ASTM, New York, 2002.
3. .Miksa De Sorgo, "Measurement, Significance and Application of Thermal Properties of Thermal Interface Materials Using ASTM D 5470," Proceedings of 19th IEEE Semiconductor Thermal Measurement and Management Symposium, San Jose, CA, March 11-13, pp. 119 -122, 2003.
4. Clemens J.M. Lasance, "The Urgent Need for Widely-Accepted Test Methods for Thermal Interface Materials," Proceedings of 19th IEEE Semiconductor Thermal Measurement and Management Symposium, San Jose, CA, March 11-13, pp. 123 - 128, 2003.
5. S.K. Parihar and N.T. Wright, "Thermal Contact Resistance at Elastomer to Metal Interfaces," International Communications Heat Mass Transfer, vol. 24, pp. 1083 - 1092, 1997.
6. .B. Rauch, "Understanding the Performance Characteristics of Phase-Change Thermal Interface Materials," Proceedings of ITHERM 2000 - Seventh Intersociety Conference on Thermal and Thermomechanical Phenomena in Electronic Systems, Las Vegas, Nevada, USA, May 24-26, vol. 1, pp. 42—47, 2000.
7. .G.L. Solbrekken, C. Chia-Pin, B. Byers, and D. Reichenbacher, "The Development of a Tool to Predict Package Level Thermal Interface Material Performance," Proceedings of ITHERM 2000 - Seventh Intersociety Conference on Thermal and Thermomechanical Phenomena in Electronic Systems, Las Vegas, NV, USA, May 24-26, vol. 1, pp. 48—54, 2000.
8. .R.S. Prasher, P. Koning, J. Shipley, and A. Devpura, "Effect of Particle Volume Fraction on the Thermal Conductivity and Mechanical Rigidity of Particle-Laden Polymeric Thermal Interface Material," Proceedings of the 2001 ASME International Mechanical Engineering Congress and Exposition, New York, NY, USA, July 10, vol. 369, pp. 67-73, 2001.
9. .I. Savija, J.R. Culham, and M.M. Yovanovich, "Effective Thermophysical Properties of Thermal Interface Materials: Part I Definitions and Models," Proceedings of ASME/Interpack 2003-35088, 2003 International Electronic Packaging Technical Conference and Exhibition, Maui, HI, USA, July 6-11, pp. 189 - 200, 2003.
10. Savija, J.R. Culham, and M.M. Yovanovich, "Effective Thermophysical Properties of Thermal Interface Materials: Part II Experiments and Data," Proceedings of ASME/Interpack 2003-35264, 2003 International Electronic Packaging Technical Conference and Exhibition, Maui, Hawaii, USA, July 6-11, pp. 567 - 573, 2003.
11. .Savija, "Method for Determining Thermophysical Properties of Thermal Interface Materials," M.S. thesis, Department of Mechanical Engineering, University of Waterloo, Waterloo, Ontario, Canada, 2002.
12. .J.R. Culham, P. Teertstra, I. Savija, and M.M Yovanovich., "Design, Assembly and Commissioning of a Test Apparatus for Characterizing Thermal Interface Materials," Proceedings of Eighth Intersociety Conference on Thermal and Thermomechanical Phenomena in Electronic Systems, San Diego, CA, USA, May 30-Jun 1, pp. 128 - 135, 2002.
13. Hamamatsu, "One-Dimensional PSD," KPSD1002E02, www.hamamatsu.com, 2001.
14. .Jack Philip Holman, Experimental Methods for Engineers, McGraw-Hill, New York, 1994.
15. R. Andrew Smith, "In-Situ Thickness Method of Measuring Thermo-Physical Properties of Polymer-Like Thermal Interface Materials," M.S. thesis, Department of Mechanical Engineering, University of Waterloo, Waterloo, Ontario, Canada, 2004.